

Absolute cryogenic radiometer and solid-state trap detectors for IR power scales down to 1 pW with 0.1% uncertainty

Adriaan C Carter¹, Solomon I Woods², Stephen M Carr², Timothy M Jung² and Raju U Datla¹

¹ National Institute of Standards and Technology, NIST, Gaithersburg, MD, USA

² Jung Research and Development Corp., Washington, DC, USA

E-mail: adriaan.carter@nist.gov

Received 15 October 2008

Published 2 June 2009

Online at stacks.iop.org/Met/46/S146

Abstract

Commercially available absolute cryogenic radiometers (ACRs) have combined uncertainties that grow rapidly above 1% ($k = 1$) at power levels below 10 nW. There are solid state detectors, however, used in sensors and radiometers that cannot be calibrated at levels as high as 10 nW because they begin to saturate. For this reason new detector-based standards are being developed to provide the low-background infrared calibration community with absolute traceability to powers down to 1 pW with $\sim 0.1\%$ ($k = 1$) combined uncertainty. The scale will be established using an ACR with a combined uncertainty of the order of 1 fW and a trap detector based on arsenic-doped silicon blocked impurity band devices with similar noise floor performance.

(Some figures in this article are in colour only in the electronic version)

1. Introduction

The Low-Background Infrared (LBIR) Facility at the National Institute of Standards and Technology (NIST) maintains the US standard for infrared power measurements in low-background environments from 20 K to 80 K [1] using absolute cryogenic radiometers (ACRs) [2]. To easily disseminate the ACR-based standard, LBIR uses a transfer radiometer which relies upon blocked impurity band (BIB) detectors made with an arsenic-doped silicon IR-active layer. Although the BIB detectors can make measurements with sensitivity at the level of 1 fW, the absolute traceability to the ACR-based standard is limited to powers of the order of 10 pW and greater at present.

Infrared measurement systems requiring a low-background environment include space-based sensors that are designed to detect ballistic warheads coming over the Earth's horizon and ground- and space-based astronomical telescopes. These systems require measurements with accuracy in the femtowatt range, so any traceability to the present-day ACR standard requires extrapolation or 'boot-strapping' over many orders

of magnitude in power. Extrapolation to absolute traceability often leads to unacceptably large uncertainties for the end user. To address this problem the LBIR Facility at NIST is developing a pair of advanced detectors which will be used to disseminate IR power calibrations down to 1 pW with a combined uncertainty of about 0.1% ($k = 1$).

The first detector will be an ACR with a fW-level noise floor ('pW-ACR') and will be used to provide absolute traceability through electrical substitution power measurement methods. This ACR-based standard will be transferred to a second detector, which will be a trap detector [3–5] formed from two large area, high quantum efficiency (QE) BIB devices ('BIB trap'). The trap detector will have femtowatt sensitivity and a flat spectral response with the total QE near 100% in the wavelength range from 4 μm to 28 μm . Intercomparison of the two detectors at 2 K will be used to calibrate the BIB trap in an environment where the sensitivity of the pW-ACR is optimal. The BIB trap will be a more 'user-friendly' detector than the pW-ACR, allowing for calibrations at user sites and at higher background temperatures.

Table 1. Comparison of critical construction and performance parameters between the current ACRII and the planned pW-ACR.

Receiver cavity property	ACRII	pW-ACR
Cone angle/deg	30	30
Cone diameter/cm	2.5	0.4
Responsivity/K mW ⁻¹	210	~30 000
Time constant/s	17	~50
Noise floor/pW	>8	~0.001
Maximum power/nW	~10 ⁵	~20

2. High sensitivity ACR (pW-ACR)

The pW-ACR design is based on an ACRII model that is currently in use at the LBIR Facility [6], with various improvements to increase radiometer sensitivity. Table 1 shows the most relevant performance differences between the currently used ACRII and the planned pW-ACR. Direct improvements in sensitivity are made by employing a more sensitive thermometer on the ACR receiver cavity, weakening the heat link from the receiver cavity to the (second stage) heat sink and operating at a lower background temperature. The smaller cone size, which reduces its mass by a factor of about 40, allows the time constant to remain under 1 min even though the thermal conductance is more than 100 times smaller for the pW-ACR than for the ACRII.

An ultra-sensitive superconducting transition edge sensor (TES) thermometer made from high purity tin (Sn) monitored by a superconducting quantum interference device (SQUID) will measure the temperature of the pW-ACR receiver cavity. Generally, TES thermometers employ a resistive measurement of the superconducting element [7–9], but for the pW-ACR the sample will be placed in a uniform magnetic field and its magnetization measured using the SQUID. There are a number of important benefits in using this non-contact measurement technique with a variable magnetic field. First, the power dissipation in the temperature sensor will be negligible. Second, the temperature resolution for the lowest power measurements can be improved by increasing the dc magnetic field. Third, the operating temperature and power of the receiver cavity can be changed by varying the dc magnetic field, as this field can be used to tune the tin superconducting transition to any temperature below 3.7 K. The feasibility of this approach is shown in figure 1, where the critical temperature of tin is changed from its zero-field value of 3.7 K to a value of 2.5 K by applying a field of 12.7 kA m⁻¹ (160 Oe), while the sharpness of transition remains at a value of less than 30 mK.

Magnetization changes of the tin transition element are picked up by a superconducting gradiometer attached to the input coil of the SQUID. The gradiometer design protects the measurement from external magnetic signals and will allow the radiometer to be operated in electromagnetically noisy lab environments. The sensitivity of the gradiometer–SQUID circuit operating at 2.5 K can be approximated by

$$S_{\text{Power}} = (S_{\Phi}) \left(\frac{\Delta T}{\Delta \Phi} \right) (G) = (10^{-19} \text{ T m}^2) \\ \times \left(\frac{3 \times 10^{-2} \text{ K}}{2.4 \times 10^{-11} \text{ T m}^2} \right) \left(\frac{10^{-3} \text{ W}}{3 \times 10^4 \text{ K}} \right) \cong 4.2 \times 10^{-18} \text{ W},$$

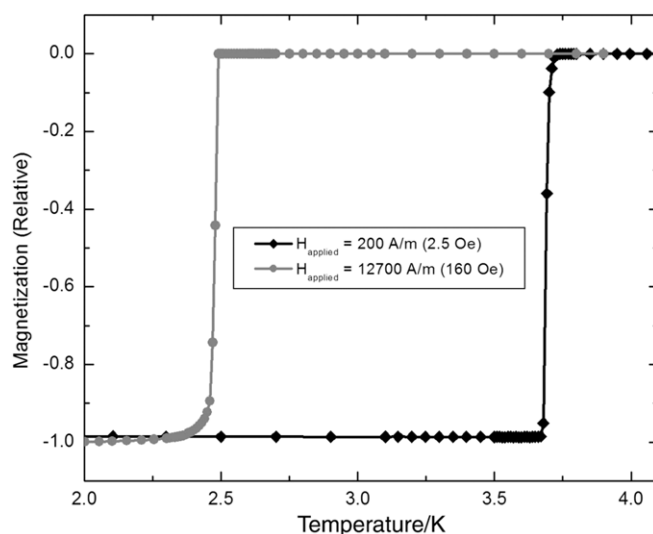


Figure 1. Magnetic measurement of the superconducting transition of a tin wire in applied dc magnetic fields of 2.5 Oe and 160 Oe. The critical temperature of the transition is reduced from about 3.7 K to 2.5 K, while the transition width remains below 30 mK.

where S_{Φ} is the dc flux sensitivity of the SQUID, ΔT is the tin transition width, $\Delta \Phi$ is the flux change seen by the SQUID over the tin superconducting transition and G is the thermal conductance of the heat link that connects the receiver cavity and the heat sink. Estimates for the SQUID parameters S_{Φ} and $\Delta \Phi$ are based on measurements of a prototype SQUID–gradiometer circuit. Apart from the physical sources of noise, the potential sensitivity of the SQUID-based TES thermometer is thus at least two orders of magnitude better than required for our power measurement.

For the pW-ACR, the receiver is a conical cavity with a base diameter of about 4 mm, and its inside is painted with IR-absorbing black paint to maximize absorption. To maximize thermal conductivity and minimize heat capacity, the cone is made from 50 μm thick electroformed copper, plated with gold. Measurements with 10.6 μm radiation demonstrate an average absorption of about 0.9994 in the three receivers fabricated thus far. The heat link connecting the receiver cavity to the second stage heat sink has the dual purpose of setting an appropriate level of thermal isolation between these two elements and providing a rigid framework for holding the receiver in place. Thin-walled Kapton tubing allows for enough strength to hold the receiver cone while providing a thermal conductance of about 30 000 K mW⁻¹ for a few millimetres length [10, 11]. Figure 2 shows a photograph of the receiver cavity held in place by a thin insulating Kapton tube in a configuration used for thermal impedance measurements.

Numerous noise sources will affect the performance of the pW-ACR including the phonon noise associated with heat flowing into and out of the tin TES element, photon noise from fluctuations in blackbody radiation, Johnson noise from the resistive receiver heater, SQUID noise and noise associated with maintaining active temperature control of the receiver. The largest of these sources is estimated to be the phonon noise, which is expected to be at the femtowatt level. The phonon

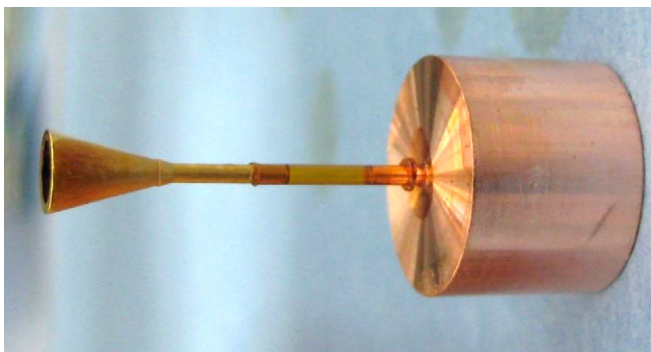


Figure 2. Photograph of a pW-ACR receiver cavity held in place by a thin Kapton tube. The receiver cone has a base diameter of 4 mm and is made from electroformed copper plated with gold. The Kapton has very low thermal conductance but is rigid enough to hold the cavity in place.

noise equivalent power can be approximated as $(4k_B GT^2)^{0.5}$, where G is the dynamic thermal conductance and T is the temperature of the tin element. For operation at 2 K and $G = (30\,000\text{ K mW}^{-1})^{-1}$, the phonon noise equivalent power is about $2.7 \times 10^{-15}\text{ W Hz}^{-0.5}$. The phonon noise contribution can be reduced by lowering the temperature of the tin, lowering the temperature of the heat sink, reducing the thermal link conductance or increasing the integration time.

For measurement of the lowest power levels the pW-ACR must be operated in a stable, 2 K background environment. Above 2 K, noise from background radiation significantly increases the overall noise floor of the instrument. The existing LBIR calibration chambers generally operate with a 15 K to 20 K environment, so transfer of the pW-ACR standard to the BIB trap detector will take place inside a pumped liquid helium cryostat at 2 K. Unlike the pW-ACR, the trap detector can be readily employed in the standard LBIR calibration chambers, while maintaining its femtowatt sensitivity. The BIB devices exhibit a steep drop in responsivity at wavelengths beyond 30 μm , making their sensitivity to blackbody radiation from a 20 K background very weak. Thus the contribution to noise from the background for the BIB trap will not change significantly between the 2 K background of the pW-ACR intercomparison cryostat and the 20 K background of the LBIR calibration chambers.

3. BIB trap detector

The BIB devices used in this study were custom-designed to maximize internal QE and minimize dark current³. BIB devices currently used as transfer detectors by the LBIR Facility exhibit the maximum total QE near 60% (with about 30% loss from reflection at the device surface), highly frequency dependent response (from etalon effects) and $D^* \approx 10^{14}\text{ cm}^2\text{ Hz}^{0.5}\text{ W}^{-1}$ from dark current at an operating temperature of 12 K. Compared with the currently used BIBs, the devices designed for the BIB trap use a thicker IR-active

³ BIB devices were fabricated by DRS Sensors and Targeting Systems, Inc. Identification of particular manufacturers in this paper does not imply endorsement by the National Institute of Standards and Technology.

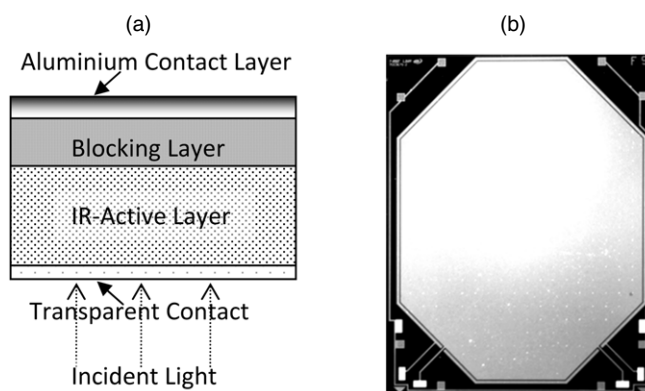


Figure 3. (a) Schematic of the layers in the BIB device structure and (b) picture of the aluminum contact layer side of a BIB device designed for a trap detector with a 3 mm entrance aperture. The approximate device dimensions are 8.5 mm \times 10.5 mm.

layer to boost QE (by increasing internal absorption within the layer) and an IR-active layer with lower defect density to lower dark current density. The IR-active layer is located right at the surface of the new BIB devices (below a thin transparent contact) in order to minimize losses and maximize internal QE. Placing the new BIBs in a trapping arrangement will catch the reflected light from the device surfaces, allowing the total QE of the trap detector to approach the internal QE of the BIB devices. The thicker IR-active layer within the devices and the trapping design will also serve to wash out the etalon effects on the detector response caused by interference from the closely spaced faces of the detectors. Figure 3 presents a picture of a trap detector designed for measurement of an $f/4$ beam with a 3 mm entrance aperture, as well as a simple schematic of the primary layers in the BIB device structure. Measurements of the low temperature reflectance and transmission of the arsenic-doped silicon IR-active layer of these new detectors imply absorption of 64% and 99% (of the non-reflected light) at 4 μm and 10 μm , respectively, for a single incidence. The BIBs have an aluminium back contact, so nearly all of the incident IR radiation executes two passes through the IR-active layer before escaping through the device face of incidence.

To maximize light collection in a simple design, the trap detector is composed of two identical BIB devices in a wedge geometry, as shown in figure 4. The design ensures that an incident $f/4$ beam, after passing through an entrance aperture, will bounce a minimum of seven times before escaping from the trap or striking an area outside the IR-active region. Two modelling programs were used to optimize the design of the trap geometry. The first calculated the minimum required device size by modelling how an incident beam would travel through a trap, allowing the wedge angle and the first bounce incidence angle to vary in order to minimize the device area. Other parameters such as aperture placement relative to the trap and device substrate extent were also taken into account in calculating the active area size. In the second program, the trapping QE (disregarding internal QE losses, which were designed to be less than 1% by the manufacturer) of the planned trap detector was calculated, accounting for light reflected out of the trap and losses at the aluminium back contacts. The largest contribution to trapping inefficiency is expected to be

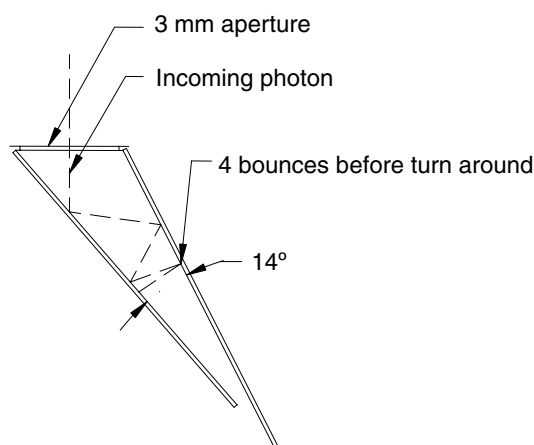


Figure 4. Schematic of the wedge design used for the BIB trap. The dotted line shows how a photon would bounce between the two devices of the trap. The design ensures that an incident $f/4$ beam will bounce a minimum of seven times before escaping from the trap.

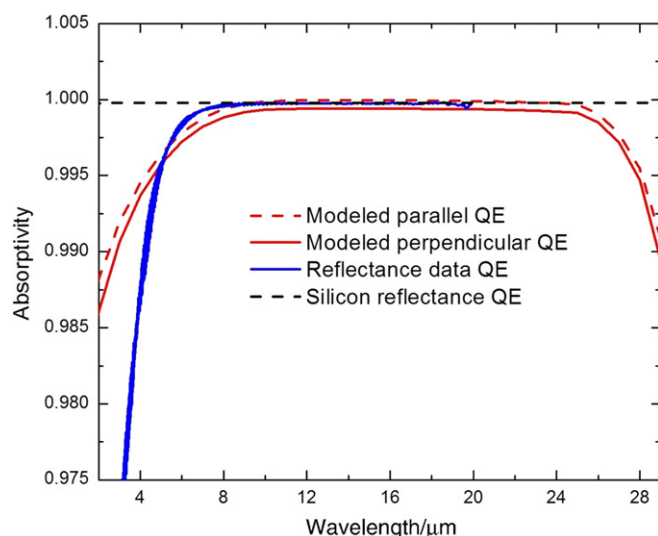


Figure 5. Trapping QE estimates from the modelled seven-bounce trap (parallel and perpendicular polarizations of incident light), from the reflectance measured on the BIB device IR-active material and from a simple model assuming a device with the surface reflectance of silicon and perfect absorption.

the loss at the aluminium back contact and is approximately given by $\xi(1 - R_{Al})$, where ξ is the transmission through the IR-active layer and R_{Al} is the reflectance of the aluminium thin film back contact. For reasonable estimates of ξ and R_{Al} , the loss at the back contacts is expected to be $<0.5\%$ for wavelengths between $4 \mu\text{m}$ and $28 \mu\text{m}$. Complete results from the trapping QE modelling are shown in figure 5 for parallel and perpendicular polarizations of incident light. Another simple estimate of trapping QE can be made by using the reflectance data taken on the IR-active material of the detector (along with reasonable estimates of the IR-active layer surface reflectance and aluminium back contact reflectance), and this result is also presented in figure 5.

The two BIB devices will be attached to Invar frames and held rigidly in the trapping geometry by a trap detector

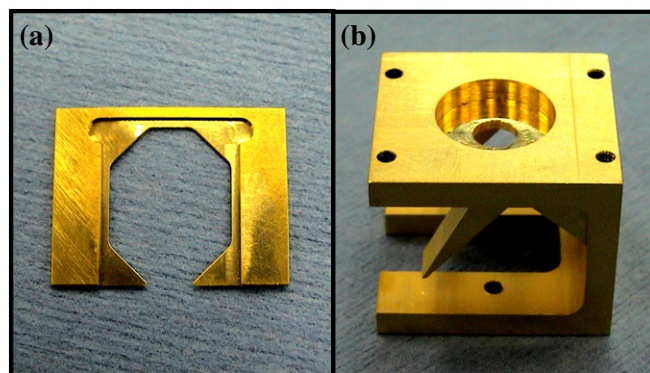


Figure 6. Photograph of the frame and mount for a 3 mm aperture trap detector. Each BIB device is attached to a frame and then the two frames are attached to the wedge of the mount. Both frame and mount are made from Invar plated with gold.

mount machined from a single piece of Invar. Figure 6 shows a photograph of the frame and mount for the 3 mm aperture trap detector. Both frame and trap mount are plated with gold, and their Invar construction should minimize the thermal contraction mismatch between the silicon-based BIBs and their mounts. Backside electrical contact and wirebonding of the devices can be accomplished in the frames before the frames are attached to the mount.

After completion of both the pW-ACR and BIB trap detector, a direct intercomparison of the two radiometers will be made at 2 K to calibrate the BIB trap. Signal from the two detectors will be compared in real time by mounting both in the same cryostat and using a translation stage to place each in turn in the path of a monochromatic or narrow-band infrared beam. Comparison will be made through a source power range of 1 pW to 20 nW and in a wavelength range from $1 \mu\text{m}$ to $30 \mu\text{m}$. Much of the hardware for the intercomparison is complete, including a custom-made integrating sphere for reducing the source power to the very low levels to be calibrated.

4. Conclusion

The LBIR Facility at NIST is well advanced in the development of a detector-based calibration system capable of performing calibrations at 1 pW of IR power with 0.1% ($k = 1$) uncertainty. The pW-ACR will serve as a new US standard for IR pW-power measurements in low background, and the BIB trap will be a transfer detector capable of disseminating this new low power calibration capability. As a transfer standard in the wavelength range from $1 \mu\text{m}$ to $30 \mu\text{m}$, the BIB trap will offer noise performance of the order of 1 fW and linearity around 0.1%, as well as a flat spectral response with the total QE near 99%. The BIB devices are also expected to offer fast response times, with a 3 dB roll-off of about 1 MHz at their warmer operating temperatures. The fast response will make the BIB trap suitable for Fourier transform spectroscopy applications.

Acknowledgments

The authors would like to thank Jinan Zeng for reflectance measurements on the pW-ACR receiver cones and Simon

Kaplan for reflection and transmission measurements on the BIB device IR-active layer.

References

- [1] Datla R U, Croarkin M C and Parr A C 1994 Cryogenic blackbody calibrations at the National Institute of Standards and Technology *J. Res. Natl Inst. Stand. Technol.* **99** 77–87
- [2] Foukal P V, Hoyt C C, Kochling H and Miller P J 1990 Cryogenic absolute radiometers as laboratory irradiance standards, remote sensing detectors, and pyroheliometers *Appl. Opt.* **29** 988–93
- [3] Zalewski E F and Duda C R 1983 Silicon photodiode device with 100% external quantum efficiency *Appl. Opt.* **22** 2867–73
- [4] Gardner J L 1994 Transmission trap detectors *Appl. Opt.* **33** 5914–8
- [5] Kubarsepp T, Karha P and Ikonen E 1997 Characterization of a polarization-independent trap detector *Appl. Opt.* **36** 2807–12
- [6] Carter A C, Lorentz S R, Jung T M and Datla R U 2005 ACR II: Improved absolute cryogenic radiometer for low background infrared calibrations *Appl. Opt.* **44** 871–5
- [7] Irwin K D 1995 An application of electrothermal feedback for high resolution cryogenic particle detection *Appl. Phys. Lett.* **66** 1998–2000
- [8] Reintsema C D, Koch J A and Grossman E N 1998 High precision electrical substitution radiometer based on superconducting-resistive-transition edge thermometry *Rev. Sci. Instrum.* **69** 152–63
- [9] Chervenak J A, Grossman E N, Reintsema C D, Irwin K D, Moseley S H and Allen C A 2001 Sub-picowatt precision radiometry using superconducting transition edge sensor bolometers *IEEE Trans. Appl. Supercond.* **11** 593–6
- [10] Barucci M, Gottardi E, Peroni I and Ventura G 2000 Low temperature thermal conductivity of Kapton and Upilex *Cryogenics* **40** 145–7
- [11] Zhang Z M, Lorentz S R, Rice J P and Datla R U 1998 Measurement of thermophysical properties of polyimide and a black paint for future development of cryogenic radiometers *Metrologia* **35** 511–5